View metadata, citation and similar papers at core.ac.uk
brought to you by CORE
provided by CERN Document Server

To appear in "Type Ia Supernovae: Theory and Cosmology"
ed. J. Truran & J. Niemeyer (Cambridge University Press), 1999

Type Ia Supernova Progenitors, Environmental Effects, and Cosmic Supernova Rates

By Ken'ichi NOMOTO[1], Hideyuki UMEDA[1], Izumi HACHISU[2], Mariko KATO[3], Chiaki KOBAYASHI[1], & Takuji TSUJIMOTO[4]

[1]Department of Astronomy, and Research Center for the Early Universe, University of Tokyo Tokyo 113-0033
[2]Department of Earth Science and Astronomy, College of Arts and Sciences, University of Tokyo, Tokyo 153-8902
[3]Department of Astronomy, Keio University, Hiyoshi, Kouhoku-ku, Yokohama 223-8521
[4]National Astronomical Observatory, Mitaka, Tokyo 181-8588

Relatively uniform light curves and spectral evolution of Type Ia supernovae (SNe Ia) have led to the use of SNe Ia as a "standard candle" to determine cosmological parameters, such as the Hubble constant, the density parameter, and the cosmological constant. Whether a statistically significant value of the cosmological constant can be obtained depends on whether the peak luminosities of SNe Ia are sufficiently free from the effects of cosmic and galactic evolutions.

Here we first review the single degenerate scenario for the Chandrasekhar mass white dwarf (WD) models of SNe Ia. We identify the progenitor's evolution and population with two channels: (1) the WD+RG (red-giant) and (2) the WD+MS (near main-sequence He-rich star) channels. In these channels, the strong wind from accreting white dwarfs plays a key role, which yields important age and metallicity effects on the evolution.

We then address the questions whether the nature of SNe Ia depends systematically on environmental properties such as metallicity and age of the progenitor system and whether significant evolutionary effects exist. We suggest that the variation of the carbon mass fraction X(C) in the C+O WD (or the variation of the initial WD mass) causes the diversity of the brightness of SNe Ia. This model can explain the observed dependence of SNe Ia brighness on the galaxy types.

Finally, applying the metallicity effect on the evolution of SN Ia progenitors, we make a prediction of the cosmic supernova rate history as a composite of the supernova rates in different types of galaxies.

1. Introduction

Type Ia supernovae (SNe Ia) are good distance indicators, and provide a promising tool for determining cosmological parameters (e.g., Branch 1998). SNe Ia have been discovered up to $z \sim 1.32$ (Gilliland et al. 1999). Both the Supernova Cosmology Project (Perlmutter et al. 1997, 1999) and the High-z Supernova Search Team (Garnavich et al. 1998; Riess et al. 1998) have suggested a statistically significant value for the cosmological constant.

However, SNe Ia are not perfect standard candles, but show some intrinsic variations in brightness. When determining the absolute peak luminosity of high-redshift SNe Ia, therefore, these analyses have taken advantage of the empirical relation existing between the peak brightness and the light curve shape (LCS). Since this relation has been obtained from nearby SNe Ia only (Phillips 1993; Hamuy et al. 1995; Riess et al. 1995), it is important to examine whether it depends systematically on environmental properties such as metallicity and age of the progenitor system.

High-redshift supernovae present us very useful information, not only to determine

cosmological parameters but also to put constraints on the star formation history in the universe. They have given the SN Ia rate at $z \sim 0.5$ (Pain 1999) but will provide the SN Ia rate history over $0 < z < 1$. With the Next Generation Space Telescope, both SNe Ia and SNe II will be observed through $z \sim 4$. It is useful to provide a prediction of cosmic supernova rates to constrain the age and metallicity effects of the SN Ia progenitors.

SNe Ia have been widely believed to be a thermonuclear explosion of a mass-accreting white dwarf (WD) (e.g., Nomoto et al. 1997a for a review). However, the immediate progenitor binary systems have not been clearly identified yet (Branch et al. 1995). In order to address the above questions regarding the nature of high-redshift SNe Ia, we need to identify the progenitors systems and examine the "evolutionary" effects (or environmental effects) on those systems.

In §2, we summarize the progenitors' evolution where the strong wind from accreting WDs plays a key role (Hachisu, Kato, & Nomoto 1996, 1999, hereafter HKN96, HKN99; Hachisu, Kato, Nomoto & Umeda 1999, HKNU99). In §3, we addresses the issue of whether a difference in the environmental properties is at the basis of the observed range of peak brightness (Umeda et al. 1999b). In §4, we make a prediction of the cosmic supernova rate history as a composite of the different types of galaxies (Kobayashi et al. 1999).

2. Progenitor's evolution and the white dwarf wind

There exist two models proposed as progenitors of SNe Ia: 1) the Chandrasekhar mass model, in which a mass-accreting carbon-oxygen (C+O) WD grows in mass up to the critical mass $M_{\rm Ia} \simeq 1.37 - 1.38 M_\odot$ near the Chandrasekhar mass and explodes as an SN Ia (e.g., Nomoto et al. 1984, 1994), and 2) the sub-Chandrasekhar mass model, in which an accreted layer of helium atop a C+O WD ignites off-center for a WD mass well below the Chandrasekhar mass (e.g., Arnett 1996). The early time spectra of the majority of SNe Ia are in excellent agreement with the synthetic spectra of the Chandrasekhar mass models, while the spectra of the sub-Chandrasekhar mass models are too blue to be comparable with the observations (Höflich & Khokhlov 1996; Nugent et al. 1997).

For the evolution of accreting WDs toward the Chandrasekhar mass, two scenarios have been proposed: 1) a double degenerate (DD) scenario, i.e., merging of double C+O WDs with a combined mass surpassing the Chandrasekhar mass limit (Iben & Tutukov 1984; Webbink 1984), and 2) a single degenerate (SD) scenario, i.e., accretion of hydrogen-rich matter via mass transfer from a binary companion (e.g., Nomoto 1982; Nomoto et al. 1994). The issue of DD vs. SD is still debated (e.g., Branch et al. 1995), although theoretical modeling has indicated that the merging of WDs leads to the accretion-induced collapse rather than SN Ia explosion (Saio & Nomoto 1985, 1998; Segretain et al. 1997).

In the SD Chandrasekhar mass model for SNe Ia, a WD explodes as a SN Ia only when its rate of the mass accretion ($\dot{M}$) is in a certain narrow range (e.g., Nomoto 1982; Nomoto & Kondo 1991). In particular, if $\dot{M}$ exceeds the critical rate $\dot{M}_{\rm b}$ in Eq.(2.1) below, the accreted matter extends to form a common envelope (Nomoto et al. 1979). This difficulty has been overcome by the WD wind model (see below). For the actual binary systems which grow the WD mass ($M_{\rm WD}$) to $M_{\rm Ia}$, the following two systems are appropriate. One is a system consisting of a mass-accreting WD and a lobe-filling, more massive, slightly evolved main-sequence (MS) or sub-giant star (hereafter "WD+MS system"). The other system consists of a WD and a lobe-filling, less massive, red-giant (hereafter "WD+RG system").

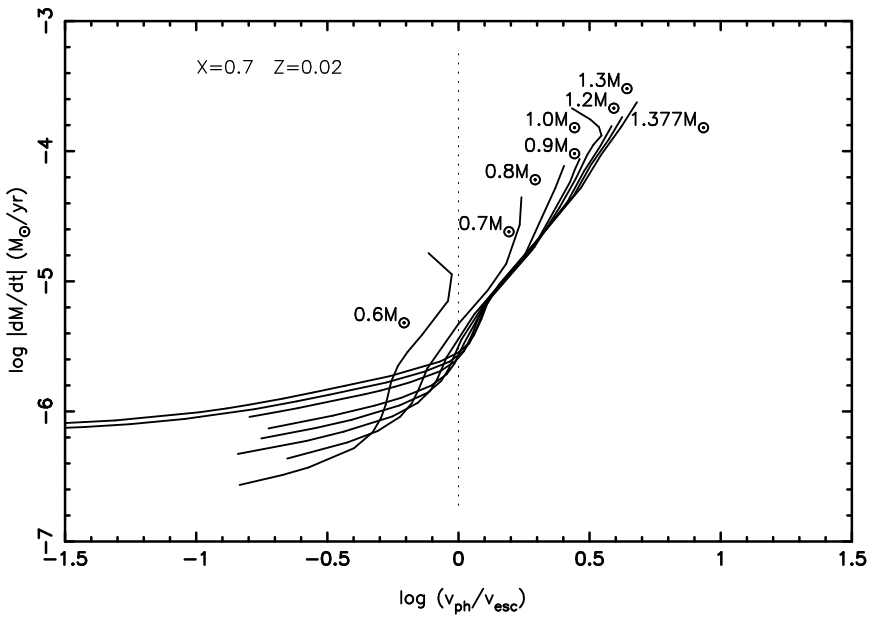

FIGURE 1. Ratio of the photospheric velocity to the escape velocity there $v_{\rm ph}/v_{\rm esc}$ is plotted against the decreasing rate of the envelope mass for WDs with masses of $0.6M_\odot$, $0.7M_\odot$, $0.8M_\odot$, $0.9M_\odot$, $1.0M_\odot$, $1.2M_\odot$, $1.3M_\odot$, and $1.377M_\odot$. We regard the wind as "strong" when the photospheric velocity exceeds the escape velocity there, i.e., $v_{\rm ph} > v_{\rm esc}$. If not, it is regarded as "weak."

2.1. *White dwarf winds*

Optically thick WD winds are driven when the accretion rate $\dot{M}$ exceeds the critical rate $\dot{M}_{\rm b}$. Here $\dot{M}_{\rm b}$ is the rate at which steady burning can process the accreted hydrogen into helium as

$$\dot{M}_{\rm b} \approx 0.75 \times 10^{-6} \left(\frac{M_{\rm WD}}{M_\odot} - 0.40 \right) M_\odot \ {\rm yr}^{-1}. \tag{2.1}$$

With such a rapid accretion, the WD envelope expands to $R_{\rm ph} \sim 0.1 R_\odot$ and the photospheric temperature decreases below $\log T_{\rm ph} \sim 5.5$. Around this temperature, the shoulder of the strong peak of OPAL Fe opacity (Iglesias & Rogers 1993) drives the radiation-driven wind (HKN96; HKN99). We plot the ratio $v_{\rm ph}/v_{\rm esc}$ between the photospheric velocity and the escape velocity at the photosphere in Figure 1 against the mass transfer rate. We call the wind *strong* when $v_{\rm ph} > v_{\rm esc}$. When the wind is strong, $v_{\rm ph} \sim 1000$ km s^{-1} being much faster than the orbital velocity.

If the wind is sufficiently strong, the WD can avoid the formation of a common envelope and steady hydrogen burning increases its mass continuously at a rate $\dot{M}_{\rm b}$ by blowing the extra mass away in a wind. When the mass transfer rate decreases below this critical value, optically thick winds stop. If the mass transfer rate further decreases below ~ 0.5 $\dot{M}_{\rm b}$, hydrogen shell burning becomes unstable to trigger very weak shell flashes but still burns a large fraction of accreted hydrogen.

The steady hydrogen shell burning converts hydrogen into helium atop the C+O core and increases the mass of the helium layer gradually. When its mass reaches a certain value, weak helium shell flashes occur. Then a part of the envelope mass is blown off but a large fraction of He can be burned to C+O (Kato & Hachisu 1999) to increase the WD

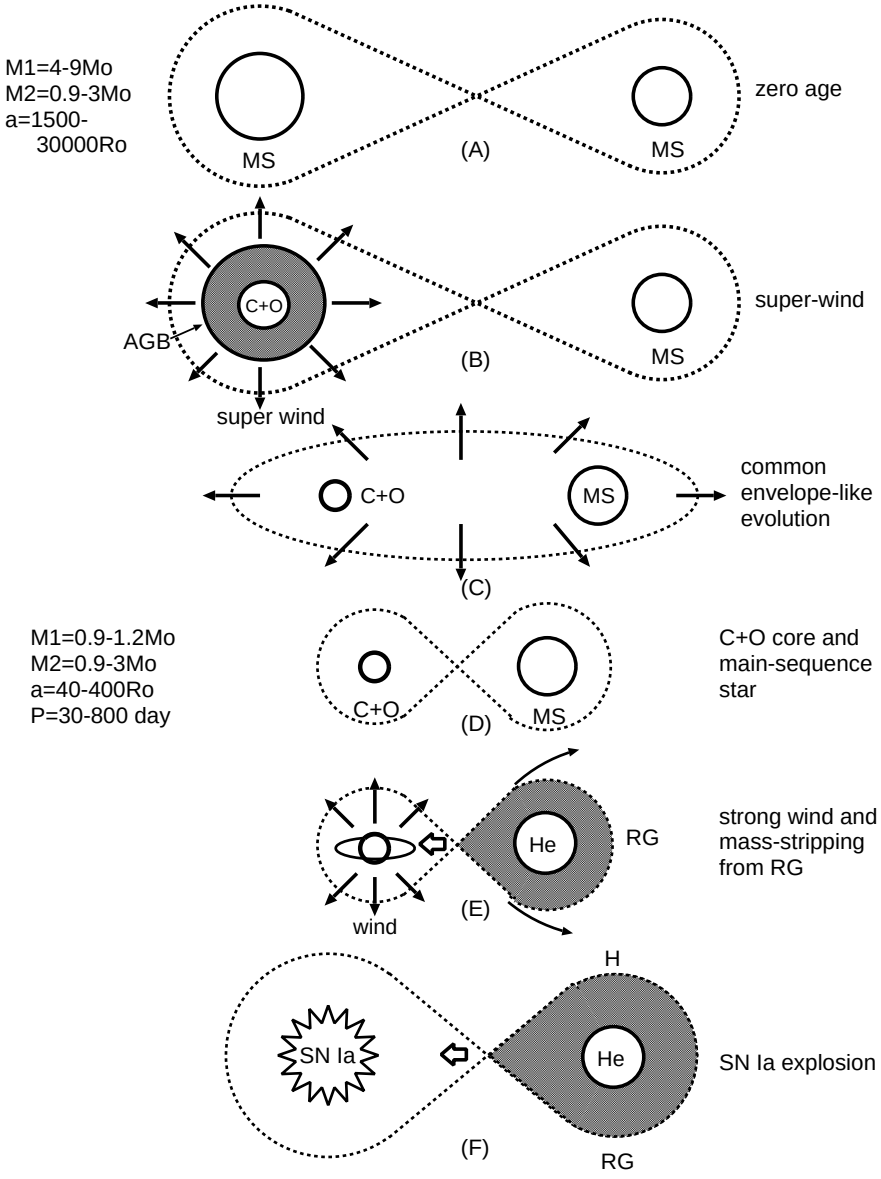

FIGURE 2. An illustration of the WD+RG (symbiotic) channel to Type Ia supernovae.

mass. In this way, Thus strong winds from the accreting WD play a key role to increase the WD mass to $M_{\rm Ia}$.

2.2. *WD+RG system*

This is a symbiotic binary system consisting of a white dwarf (WD) and a low mass red-giant (RG). A full evolutionary path of the WD+RG system from the zero age main-sequence stage (*stage A*) to the SN Ia explosion (*stage F*) is as follows.

(A) Zero age main-sequence.

(B) The primary has evolved first to become an asymptotic giant branch (AGB) star and blows a slow wind (or a super wind) at the end of the AGB evolution.

(C) If the superwind from the AGB star is as fast as or slower than the orbital velocity, the wind outflowing from the system takes away the orbital angular momentum effectively. As a result the wide binary shrinks greatly (by about a factor of ten or more) to become a close binary. This is a similar process to the common envelope evolution.

(D) Then the AGB star undergoes a common envelope evolution. The AGB star forms a C+O WD, and the initial secondary remains a main-sequence star (MS).

(E) The initial secondary evolves to a red-giant (RG) forming a helium core and fills up its inner critical Roche lobe. Mass transfer begins. The WD component blows a strong wind and the winds can stabilize the mass transfer even if the RG component has a deep convective envelope.

(F) The WD component has grown in mass to $M_{\rm Ia}$ and explodes as a Type Ia supernova.

The occurrence frequency of SNe Ia through this channel is much larger than the earlier scenario, because of the following two evolutionary processes, which have not considered before.

(1) Because of the AGB wind at stage C, the WD + RG close binary can form from a wide binary even with such a large initial separation as $a_i \lesssim 40,000 R_\odot$. Our earlier estimate (HKN96) is constrained by $a_i \lesssim 1,500 R_\odot$.

(2) When the RG fills its inner critical Roche lobe, the WD undergoes rapid mass accretion and blows a strong optically thick wind. Our earlier analysis has shown that the mass transfer is stabilized by this wind only when the mass ratio of RG/WD is smaller than 1.15. Our new finding is that the WD wind can strip mass from the RG envelope, which could be efficient enough to stabilize the mass transfer even if the RG/WD mass ratio exceeds 1.15. If this mass-stripping effect is strong enough, though its efficiency $\eta_{\rm eff}$ is subject to uncertainties, the symbiotic channel can produce SNe Ia for a much (ten times or more) wider range of the binary parameters than our earlier estimation.

With the above two new effects (1) and (2), the WD+RG (symbiotic) channel can account for the inferred rate of SNe Ia in our Galaxy. The immediate progenitor binaries in this symbiotic channel to SNe Ia may be observed as symbiotic stars, luminous supersoft X-ray sources, or recurrent novae like T CrB or RS Oph, depending on the wind status.

2.3. *WD+MS system*

In this scenario, a C+O WD is originated, not from an AGB star with a C+O core, but from a red-giant star with a helium core of $\sim 0.8 - 2.0 M_\odot$. The helium star, which is formed after the first common envelope evolution, evolves to form a C+O WD of $\sim 0.8 - 1.1 M_\odot$ with transferring a part of the helium envelope onto the secondary main-sequence star.

As an example for this system, let us consider a pair of $7 M_\odot + 2.5 M_\odot$ with the initial separation of $a_i \sim 50 - 600 R_\odot$. The binary evolves to SN Ia through the following stages (stages A-F in Figure 3 and G in HKNU99):

(1) stage A-C: When the mass of the helium core grows to $1.0 M_\odot < M_{1,{\rm He}} < 1.4 M_\odot$, the primary fills its Roche lobe and the binary undergoes a common envelope evolution.

(2) stage C-D: After the common envelope evolution, the system consists of a helium star and a main-sequence star with a relatively compact separation of $a_f \sim 3 - 40\ R_\odot$ and $P_{\rm orb} \sim 0.4 - 20$ d.

(3) stage D: The helium star contracts and ignites central helium burning to become a helium main-sequence star. The primary stays at the helium main-sequence for $\sim 1 \times 10^7$ yr.

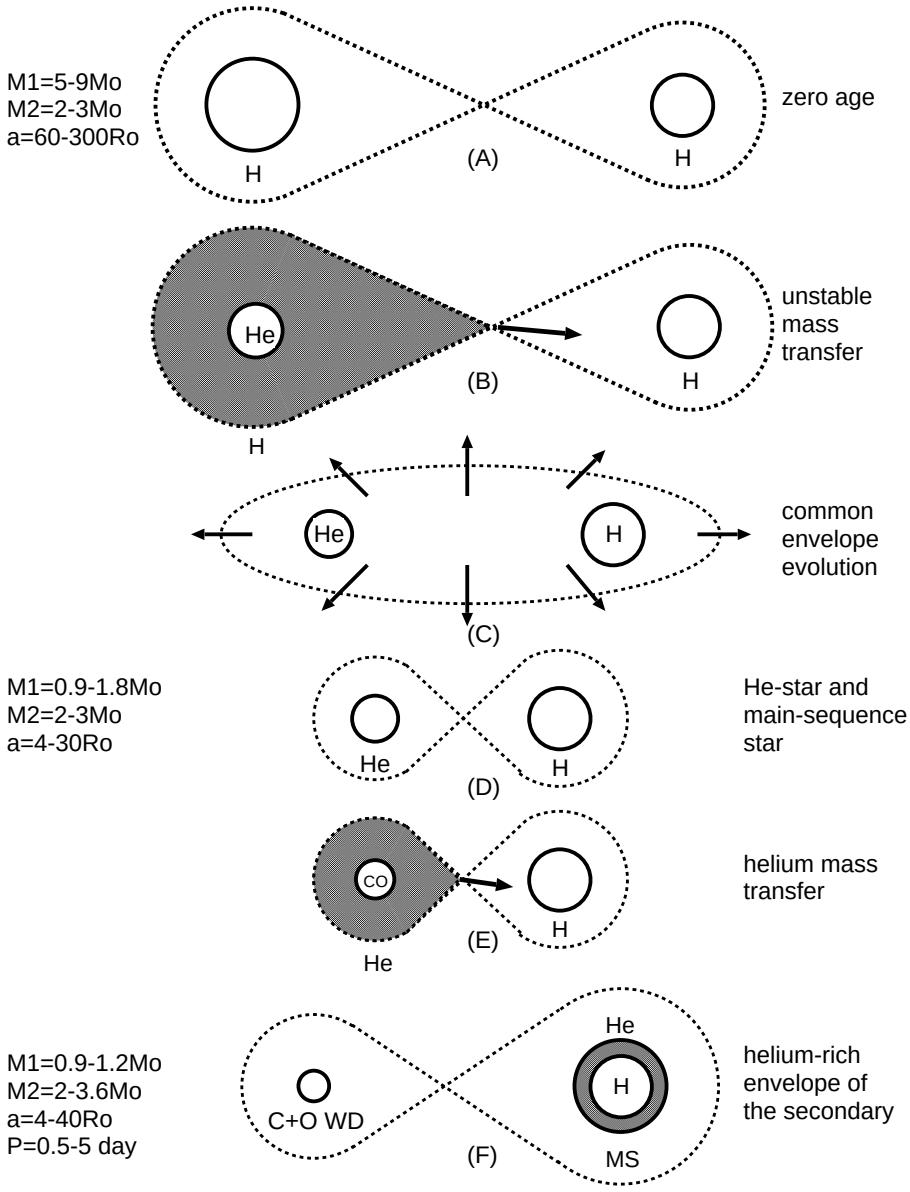

FIGURE 3. An illustration of the WD+MS channel to Type Ia supernovae through the common envelope evolution to the helium matter transfer.

(4) stage E: After helium exhaustion, a carbon-oxygen core develops. When the core mass reaches $0.9 - 1.0 M_\odot$, the helium star evolves to a red-giant and fills again its inner critical Roche lobe. Almost pure helium is transferred to the secondary because the mass transfer is stable for the mass ratio $q = M_1/M_2 < 0.79$. The mass transfer rate is as large as $\sim 1 \times 10^{-5} M_\odot$ yr^{-1} but the mass-receiving main-sequence star ($\sim 2 - 3 M_\odot$) does not expand for such a low rate.

(5) stage F: The secondary has received $0.1 - 0.4 M_\odot$ (almost) pure helium and, as a result, it becomes a helium-rich star as observed in the recurrent nova U Sco. The

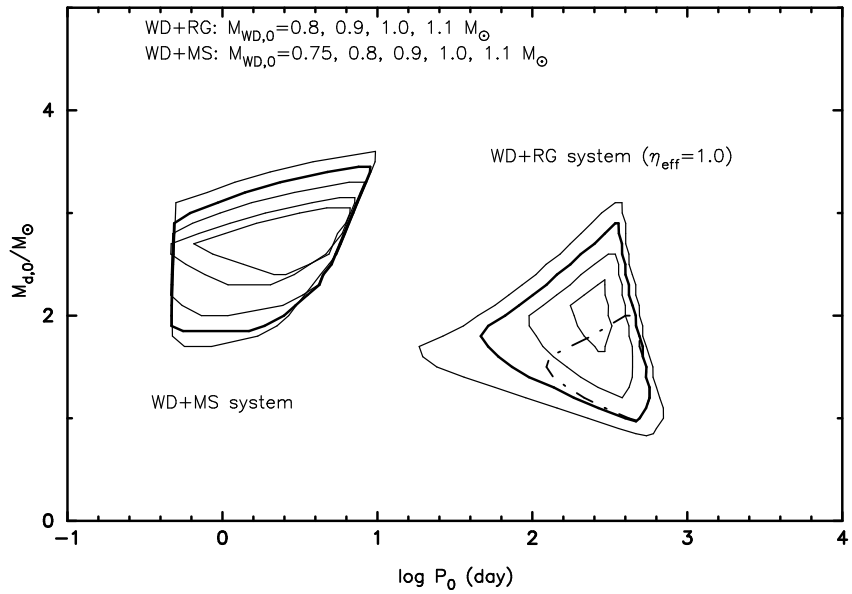

FIGURE 4. The region to produce SNe Ia in the $\log P_0 - M_{\rm d,0}$ plane for five initial white dwarf masses of $0.75M_\odot$, $0.8M_\odot$, $0.9M_\odot$, $1.0M_\odot$ (heavy solid line), and $1.1M_\odot$. The region of $M_{\rm WD,0} = 0.7M_\odot$ almost vanishes for both the WD+MS and WD+RG systems, and the region of $M_{\rm WD,0} = 0.75M_\odot$ vanishes for the WD+RG system. Here, we assume the stripping efficiency of $\eta_{\rm eff} = 1$. For comparison, we show only the region of $M_{\rm WD,0} = 1.0M_\odot$ for a much lower efficiency of $\eta_{\rm eff} = 0.3$ by a dash-dotted line.

primary becomes a C+O WD. The separation and thus the orbital period gradually increases during the mass transfer phase. The final orbital period becomes $P_{\rm orb} \sim 0.5-40$ d.

(6) stage G: The white dwarf accretes hydrogen-rich, helium-enhanced matter from a lobe-filling, slightly evolved companion at a critical rate and blows excess matter in the wind. The white dwarf grows in mass to $M_{\rm Ia}$ and explodes as an SN Ia.

This evolutionary path provides a much wider channel to SNe Ia than previous scenarios. A part of the progenitor systems are identified as the luminous supersoft X-ray sources (van den Heuvel et al. 1992) during steady H-burning (but without wind to avoid extinction), or the recurrent novae like U Sco if H-burning is weakly unstable. Actually these objects are characterized by the accretion of helium-rich matter.

2.4. *Realization Frequency*

For an immediate progenitor system WD+RG of SNe Ia, we consider a close binary initially consisting of a C+O WD with $M_{\rm WD,0} = 0.6 - 1.2M_\odot$ and a low-mass red-giant star with $M_{\rm RG,0} = 0.7 - 3.0M_\odot$ having a helium core of $M_{\rm He,0} = 0.2 - 0.46M_\odot$ (stage E). The initial state of these immediate progenitors is specified by three parameters, i.e., $M_{\rm WD,0}$, $M_{\rm RG,0} = M_{\rm d,0}$, and the initial orbital period P_0 ($M_{\rm He,0}$ is determined if P_0 is given).

We follow binary evolutions of these systems and obtain the parameter range(s) which can produce an SN Ia. In Figure 4, the region enclosed by the thin solid line produces SNe Ia for several cases of the initial WD mass, $M_{\rm WD,0} = 0.75$ - $1.1\ M_\odot$. For smaller $M_{\rm WD,0}$,

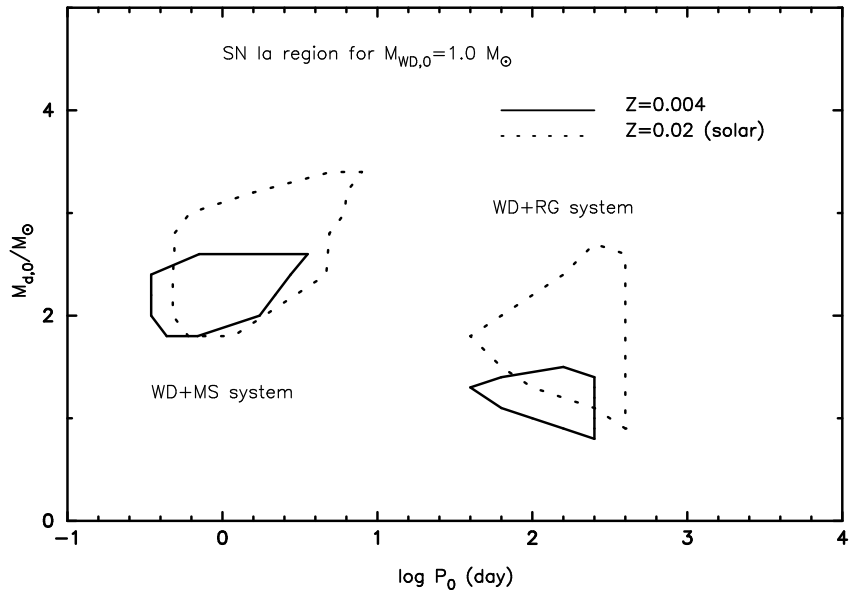

FIGURE 5. The regions of SNe Ia is plotted in the initial orbital period vs. the initial companion mass diagram for the initial WD mass of $M_{\rm WD,0} = 1.0 M_\odot$. The dashed and solid lines represent the cases of solar abundance ($Z = 0.02$) and much lower metallicity of $Z = 0.004$, respectively. The left and the right regions correspond to the WD+MS and the WD+RG systems, respectively.

the wind is weaker, so that the SN Ia region is smaller. The regions of $M_{\rm WD,0} = 0.6 M_\odot$ and $0.7 M_\odot$ vanish for both the WD+MS and WD+RG systems.

In the outside of this region, the outcome of the evolution at the end of the calculations is not an SN Ia but one of the followings:

(i) Formation of a common envelope for too large $M_{\rm d}$ or $P_0 \sim$ day, where the mass transfer is unstable at the beginning of mass transfer.

(ii) Novae or strong hydrogen shell flash for too small $M_{\rm d,0}$, where the mass transfer rate becomes below $10^{-7}\ M_\odot\ {\rm yr}^{-1}$.

(iii) Helium core flash of the red giant component for too long P_0, where a central helium core flash ignites, i.e., the helium core mass of the red-giant reaches $0.46 M_\odot$.

(iv) Accretion-induced collapse for $M_{\rm WD,0} > 1.2 M_\odot$, where the central density of the WD reaches $\sim 10^{10}$ g cm^{-3} before heating wave from the hydrogen burning layer reaches the center. As a result, the WD undergoes collapse due to electron capture without exploding as an SN Ia (Nomoto & Kondo 1991).

It is clear that the new region of the WD+RG system is not limited by the condition of $q < 1.15$, thus being ten times or more wider than the region of HKN96's model (depending on the the stripping efficiency of $\eta_{\rm eff}$).

The WD+MS progenitor system can also be specified by three initial parameters: the initial C+O WD mass $M_{\rm WD,0}$, the mass donor's initial mass $M_{\rm d,0}$, and the orbital period P_0. For $M_{\rm WD,0} = 1.0 M_\odot$, the region producing an SN Ia is bounded by $M_{\rm d,0} = 1.8 - 3.2 M_\odot$ and $P_0 = 0.5 - 5$ d as shown by the solid line in Figure 4. The upper and lower bounds are respectively determined by the common envelope formation (i) and nova-like explosions (ii) as above. The left and right bounds are determined by the minimum and maximum radii during the main sequence of the donor star (HKNU99).

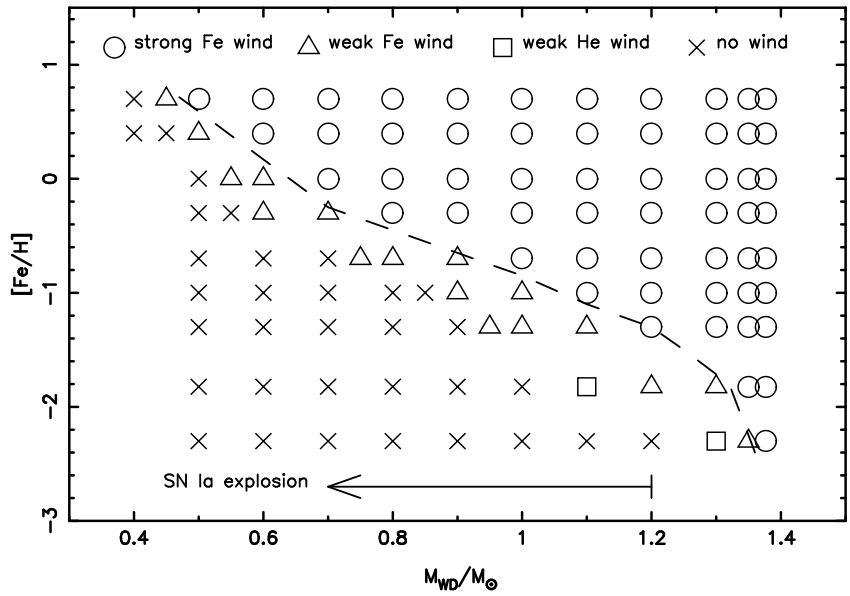

FIGURE 6. WD mass vs. metallicity diagram showing the metallicity dependence of optically thick winds We regard the wind as "strong" if the wind velocity at the photosphere exceeds the escape velocity but "weak" if the wind velocity is lower than the escape velocity. The term of "He" or "Fe" wind denotes that the wind is accelerated by the peak of iron lines near $\log T(\mathrm{K}) \sim 5.2$ or of helium lines near $\log T(\mathrm{K}) \sim 4.6$. The dashed line indicates the demarcation between the "strong" wind and the "weak" wind.

We estimate the rate of SNe Ia originating from these channels in our Galaxy by using equation (1) of Iben & Tutukov (1984). The realization frequencies of SNe Ia through the WD+RG and WD+MS channels are estimated as ~ 0.0017 yr^{-1} (WD+RG) and ~ 0.001 yr^{-1} (WD+MS), respectively. The total SN Ia rate of the WD+MS/WD+RG systems becomes ~ 0.003 yr^{-1}, which is close enough to the inferred rate of our Galaxy.

2.5. *Low metallicity inhibition of type Ia supernovae*

In the above SN Ia progenitor model, the accreting WD blows a strong wind to reach the Chandrasekhar mass limit. If the iron abundance of the progenitors is as low as $[\mathrm{Fe/H}] \lesssim -1$, then the wind is too weak for SNe Ia to occur.

In this model, an interesting metallicity effect has been found (Kobayashi et al. 1998; Hachisu & Kato 1999). The wind velocity is higher for larger $M_{\rm WD}$ and larger Fe/H because of higher luminosity and larger opacity, respectively. In order to blow sufficiently strong wind ($v_{\rm w} > v_{\rm esc}$), $M_{\rm WD}$ should exceed a certain mass $M_{\rm w}$ (Fig. 1). As seen from the dashed line in Figure 6, $M_{\rm w}$ is larger for lower metallicity; e.g., $M_{\rm w} = 0.65$, 0.85, and 0.95 $M_\odot$ for $Z = 0.02$, 0.01, and 0.004, respectively. In order for a WD to grow its mass at $\dot{M} > \dot{M}_{\rm b}$, its initial mass $M_{\rm WD,0}$ should exceed $M_{\rm w}$. In other words, $M_{\rm w}$ is the metallicity-dependent minimum $M_{\rm WD,0}$ required for a WD to become an SN Ia.

2.6. *Possible detection of hydrogen*

In our scenario, the WD winds form a circumstellar envelope around the binary systems prior to the explosion, which may emit X-rays, radio, and Hα lines by shock heating when the ejecta collide with the circumstellar envelope. The mass accretion rate in the

present models is still as high as $1 \times 10^{-6}\ M_\odot\ \mathrm{yr}^{-1}$ for some of the white dwarfs near the Chandrasekhar limit, so that such a white dwarf explode in the strong wind phase.

Our strong wind model of case P1 predicts the presence of circumstellar matter around the exploding white dwarf. Whether such a circumstellar matter is observable depends on its density. The wind mass loss rate from the white dwarf near the Chandrasekhar limit is as high as $\dot{M} \sim 1 \times 10^{-8} - 1 \times 10^{-7}\ M_\odot\ \mathrm{yr}^{-1}$ and the wind velocity is $v = 1000$ km s^{-1}. Despite the relatively high mass loss rate, the circumstellar density is not so high because of the high wind velocity. For steady wind, the density is expressed by $\dot{M}/v\ (= 4\pi r^2 \rho)$. Normalized by the typical red-giant wind velocity of 10 km s^{-1}, the density measure of our white dwarf wind is given as $\dot{M}/v_{10} \sim 1 \times 10^{-10} - 1 \times 10^{-9}\ M_\odot$ yr^{-1}, where $v_{10} = v/10$ km s^{-1}.

Behind the red-giant, matter stripped from the red-giant component forms a much dense circumstellar tail. Its rate is as large as $\sim 1 \times 10^{-7} M_\odot$ yr^{-1} with the velocity of ~ 100 km s^{-1}. The density measure of the dense red-giant wind thus formed is $\dot{M}/v_{10} \sim 1 \times 10^{-8}\ M_\odot$ yr^{-1}.

Further out, circumstellar matter is produced from the wind from the red-giant companion, which is too far away to cause significant circumstellar interaction.

For some cases, winds from the WD have stopped before the explosion. Therefore, circumstellar matter is dominated by the wind from the red-giant companion whose velocity is as low as ~ 10 km s^{-1}.

At SN Ia explosion, ejecta would collide with the circumstellar matter, which produces shock waves propagating both outward and inward. At the shock front, particle accelerations take place to cause radio emissions. Hot plasmas in the shocked materials emit thermal X-rays. The circumstellar matter ahead of the shock is ionized by X-rays and produce recombination Hα emissions (Cumming et al. 1996). Such an interaction has been observed in Type Ib, Ic, and II supernovae, most typically in SN 1993J (e.g., Suzuki & Nomoto 1995 and references therein).

For SNe Ia, several attempts have been made to detect the above signature of circumstellar matter. There has been no radio and X-ray detections so far. The upper limit set by X-ray observations of SN 1992A is $\dot{M}/v_{10} = (2-3) \times 10^{-6}\ M_\odot$ yr^{-1} (Schlegel & Petre 1993). Radio observations of SN 1986G have provided the most strict upper limit to the circumstellar density as $\dot{M}/v_{10} = 1 \times 10^{-7}\ M_\odot\ \mathrm{yr}^{-1}$ (Eck et al. 1995). This is still $10 - 100$ times higher than the density predicted for the white dwarf wind. If the WD wind has ceased and the wind mass loss rate from the red-giant is significantly higher than $1 \times 10^{-7}\ M_\odot\ \mathrm{yr}^{-1}$, radio detection could be possible for very nearby SNe Ia as close as SN 1986G. (Note also that SN 1986G is not a typical SN Ia but a subluminous SN Ia.)

For Hα emissions, Branch et al. (1983) noted a small, narrow emission feature at the rest wavelength of Hα, which is blueshifted by 1800 km s^{-1} from the local interstellar Ca II absorption. Though this feature was not observed 5 days later, such high velocity hydrogen is expected from the white dwarf wind model. For SN 1994D, Cumming et al. (1996) obtained the upper limit of $\dot{M}/v_{10} = 6 \times 10^{-6}\ M_\odot\ \mathrm{yr}^{-1}$. Further attempts to detect Hα emissions are highly encouraged.

3. The origin of diversity of SNe Ia and environmental effects

There are some observational indications that SNe Ia are affected by their environment. The most luminous SNe Ia seem to occur only in spiral galaxies, while both spiral and elliptical galaxies are hosts for dimmer SNe Ia. Thus the mean peak brightness is dimmer in ellipticals than in spiral galaxies (Hamuy et al. 1996). The SNe Ia rate per

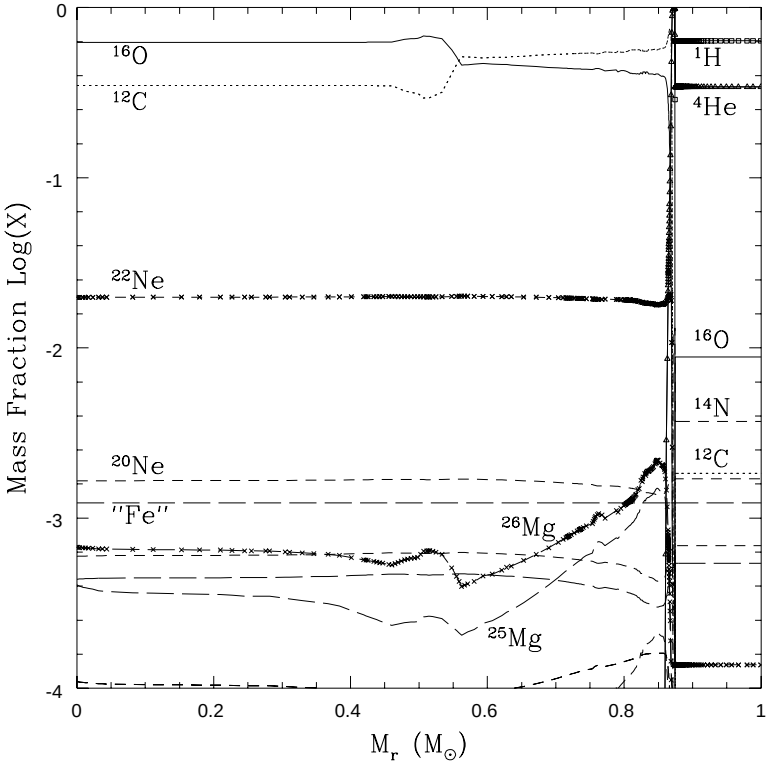

FIGURE 7. Abundances in mass fraction in the inner core of the 6 $M_\odot$ star for $Y = 0.2775$ and $Z = 0.02$ at the end of the second dredge-up.

unit luminosity at the present epoch is almost twice as high in spirals as in ellipticals (Cappellaro et al. 1997). Moreover, Wang et al. (1997) and Riess et al. (1999) found that the variation of the peak brightness for SNe located in the outer regions in galaxies is smaller.

Höflich et al. (1998, 1999) examined how the initial composition of the WD (metallicity and the C/O ratio) affects the observed properties of SNe Ia. Umeda et al. (1999a) obtained the C/O ratio as a function of the main-sequence mass and metallicity of the WD progenitors. Umeda et al. (1999b) suggested that the variation of the C/O ratio is the main cause of the variation of SNe Ia brightness, with larger C/O ratio yielding brighter SNe Ia. We will show that the C/O ratio depends indeed on environmental properties, such as the metallicity and age of the companion of the WD, and that our model can explain most of the observational trends discussed above. We then make some predictions about the brightness of SN Ia at higher redshift.

3.1. *C/O ratio in WD progenitors*

In this section we discuss how the C/O ratio in the WD depends on the metallicity and age of the binary system. The C/O ratio in C+O WDs depends primarily on the main-sequence mass of the WD progenitor and on metallicity.

We calculated the evolution of intermediate-mass ($3 - 9M_\odot$) stars for metallicity Z=0.001 – 0.03. In the ranges of stellar masses and Z considered in this paper, the most important metallicity effect is that the radiative opacity is smaller for lower Z. Therefore, a star with lower Z is brighter, thus having a shorter lifetime than a star with

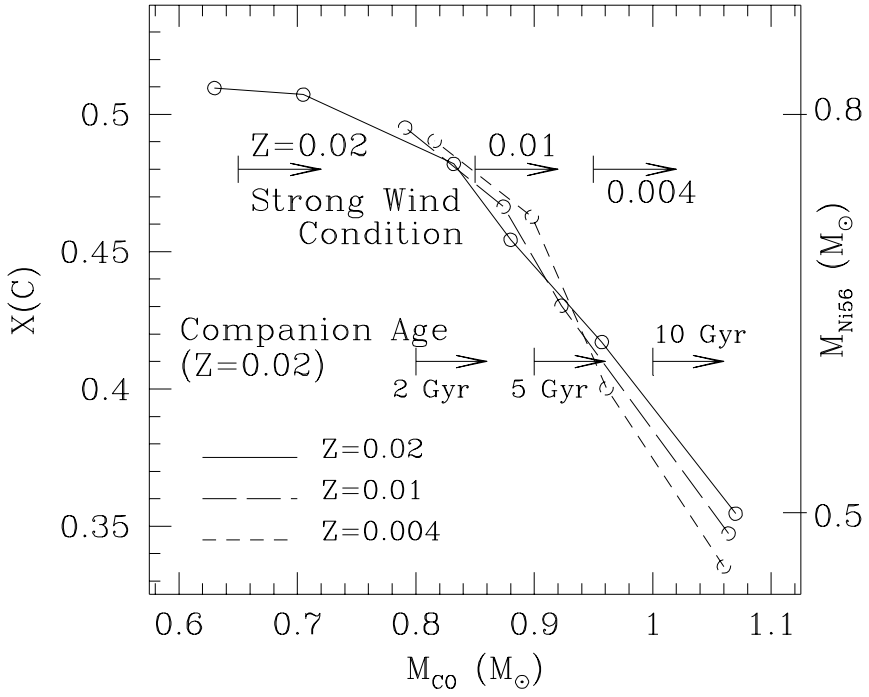

FIGURE 8. The total ^{12}C mass fraction included in the convective core of mass, $M = 1.14 M_\odot$, just before the SN Ia explosion as a function of the C+O core mass before the onset of mass accretion, $M_{\rm CO}$. The lower bounds of $M_{\rm CO}$ obtained from the age effects and the conditions for strong wind to blow are also shown by arrows.

the same mass but higher Z. In this sense, the effect of reducing metallicity for these stars is almost equivalent to increasing a stellar mass.

For stars with larger masses and/or smaller Z, the luminosity is higher at the same evolutionary phase. With a higher nuclear energy generation rate, these stars have larger convective cores during H and He burning, thus forming larger He and C-O cores.

As seen in Figure 7, the central part of these stars is oxygen-rich. The C/O ratio is nearly constant in the innermost region, which was a convective core during He burning. Outside this homogeneous region, where the C-O layer grows due to He shell burning, the C/O ratio increases up to C/O $\gtrsim 1$; thus the oxygen-rich core is surrounded by a shell with C/O $\gtrsim 1$. In fact this is a generic feature in all models we calculated. The C/O ratio in the shell is C/O $\simeq 1$ for the star as massive as $\sim 7 M_\odot$, and C/O > 1 for less massive stars.

When a progenitor reaches the critical mass for the SNe Ia explosion, the central core is convective up to around 1.1 $M_\odot$. Hence the relevant C/O ratio is between the central value before convective mixing and the total C/O of the whole WD. Using the results from the C6 model (Nomoto et al. 1984), we assume that the convective region is 1.14 $M_\odot$ and for simplicity, C/O = 1 outside the C-O core at the end of second dredge-up. Then we obtain the C/O ratio of the inner part of the SNe Ia progenitors (Fig. 8).

From this figure we find three interesting trends. First, while the central C/O is a complicated function of stellar mass (Umeda et al. 1999a), as shown here the C/O ratio in the core before SNe Ia explosion is a decreasing monotonic function of mass. The

central C/O ratio at the end of second dredge-up decreases with mass for $M_{\rm ms} \gtrsim 5M_\odot$, while the ratio increases with mass for $M_{\rm ms} \gtrsim 4M_\odot$; however, the convective core mass during He burning is smaller for a less massive star, and the C/O ratio during shell He burning is larger for smaller C+O core. Hence, when the C/O ratio is averaged over 1.1 $M_\odot$ the C/O ratio decreases with mass. Second, as shown in Umeda et al. 1999, although the C/O ratio is a complicated function of metallicity and mass, the metallicity dependence is remarkably converged when the ratio is seen as a function of the C+O core mass ($M_{\rm CO}$) instead of the initial main sequence mass.

According to the evolutionary calculations for 3−9 $M_\odot$ stars by Umeda et al. (1999a), the C/O ratio and its distribution are determined in the following evolutionary stages of the close binary.

(1) At the end of central He burning in the 3−9 $M_\odot$ primary star, C/O$<$ 1 in the convective core. The mass of the core is larger for more massive stars.

(2) After central He exhaustion, the outer C+O layer grows via He shell burning, where C/O$\gtrsim$ 1 (Umeda et al. 1999a).

(3a) If the primary star becomes a red giant (case C evolution; e.g. van den Heuvel 1994), it then undergoes the second dredge-up, forming a thin He layer, and enters the AGB phase. The C+O core mass, $M_{\rm CO}$, at this phase is larger for more massive stars. For a larger $M_{\rm CO}$ the total carbon mass fraction is smaller.

(3b) When it enters the AGB phase, the star greatly expands and is assumed here to undergo Roche lobe overflow (or a super-wind phase) and to form a C+O WD. Thus the initial mass of the WD, $M_{\rm WD,0}$, in the close binary at the beginning of mass accretion is approximately equal to $M_{\rm CO}$.

(4a) If the primary star becomes a He star (case BB evolution), the second dredge-up in (3a) corresponds to the expansion of the He envelope.

(4b) The ensuing Roche lobe overflow again leads to a white dwarf of mass $M_{\rm WD,0} = M_{\rm CO}$.

(5) After the onset of mass accretion, the WD mass grows through steady H burning and weak He shell flashes, as described in the WD wind model. The composition of the growing C+O layer is assumed to be C/O=1.

(6) The WD grows in mass and ignites carbon when its mass reaches $M_{\rm Ia} = 1.367M_\odot$, as in the model C6 of Nomoto et al. (1984). Because of strong electron-degeneracy, carbon burning is unstable and grows into a deflagration for a central temperature of 8×10^8 K and a central density of 1.47×10^9 g cm^{-3}. At this stage, the convective core extends to $M_r = 1.14M_\odot$ and the material is mixed almost uniformly, as in the C6 model.

In Figure 8, we show the carbon mass fraction X(C) in the convective core of this pre-explosive WD, as a function of metallicity (Z) and initial mass of the WD before the onset of mass accretion, $M_{\rm CO}$. Figure 8 reveals that: 1) X(C) is smaller for larger $M_{\rm CO} \simeq M_{\rm WD,0}$. 2) The dependence of X(C) on metallicity is small when plotted against $M_{\rm CO}$, even though the relation between $M_{\rm CO}$ and the initial stellar mass depends sensitively on Z (Umeda et al. 1999a).

3.2. *Brightness of SNe Ia and the C/O ratio*

In the Chandrasekhar mass models for SNe Ia, the brightness of SNe Ia is determined mainly by the mass of ^{56}Ni synthesized ($M_{\rm Ni56}$). Observational data suggest that $M_{\rm Ni56}$ for most SNe Ia lies in the range $M_{\rm Ni56} \sim 0.4 - 0.8M_\odot$ (e.g. Mazzali et al. 1998). This range of $M_{\rm Ni56}$ can result from differences in the C/O ratio in the progenitor WD as follows.

In the deflagration model, a larger C/O ratio leads to the production of more nuclear

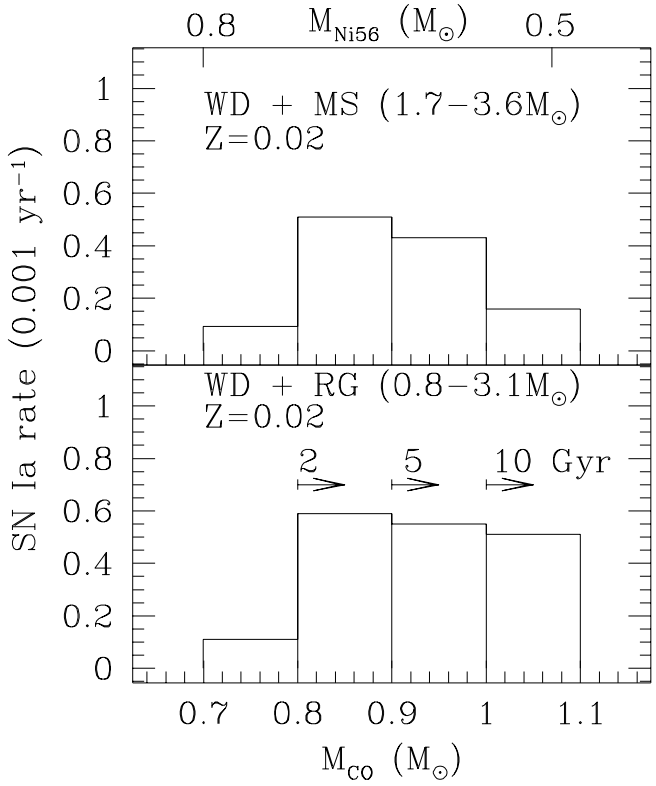

FIGURE 9. SN Ia frequency for a galaxy of mass $2 \times 10^{11} M_\odot$ as a function of $M_{\rm CO}$ for Z=0.02. For the WD+RG system, constraints from the companion's age are shown by the arrows. SNe Ia from the WD+MS system occur in spirals but not in ellipticals because of the age effect. $M_{\rm CO}$ and $M_{\rm Ni56}$ is assumed to be related as shown here.

energy and buoyancy force, thus leading to a faster propagation. The faster propagation of the convective deflagration wave results in a larger $M_{\rm Ni56}$. For example, a variation of the propagation speed by 15% in the W6 – W8 models results in $M_{\rm Ni56}$ values ranging between 0.5 and $0.7 M_\odot$ (Nomoto et al. 1984), which could explain the observations.

In the delayed detonation model, $M_{\rm Ni56}$ is predominantly determined by the deflagration-to-detonation-transition (DDT) density $\rho_{\rm DDT}$, at which the initially subsonic deflagration turns into a supersonic detonation (Khokhlov 1991). As discussed in Umeda et al. (1999b), $\rho_{\rm DDT}$ could be very sensitive to X(C), and a larger X(C) is likely to result in a larger $\rho_{\rm DDT}$ and $M_{\rm Ni56}$.

Here we postulate that $M_{\rm Ni56}$ and consequently brightness of a SN Ia increase as the progenitors' C/O ratio increases (and thus $M_{\rm WD,0}$ decreases). As illustrated in Figure 8, the range of $M_{\rm Ni56} \sim 0.5 - 0.8 M_\odot$ is the result of an X(C) range $0.35 - 0.5$, which is the range of X(C) values of our progenitor models. The X(C) – $M_{\rm Ni56}$ – $M_{\rm WD,0}$ relation we adopt is still only a working hypothesis, which needs to be proved from studies of the turbulent flame during explosion (e.g., Niemeyer & Hillebrandt 1995).

3.3. *Metallicity and age effects*

3.3.1. *Metallicity effects on the minimum* $M_{\rm WD,0}$

As mentioned in §2.5, $M_{\rm w}$ is the metallicity-dependent minimum $M_{\rm WD,0}$ for a WD to become an SN Ia (*strong wind condition* in Fig. 8). The upper bound $M_{\rm WD,0} \simeq 1.07 M_\odot$ is imposed by the condition that carbon should not ignite and is almost independent of metallicity. As shown in Figure 8, the range of $M_{\rm CO} \simeq M_{\rm WD,0}$ can be converted into a range of $X({\rm C})$. From this we find the following metallicity dependence for $X({\rm C})$:

(1) The upper bound of $X({\rm C})$, which is determined by the lower limit on $M_{\rm CO}$ imposed by the metallicity-dependent conditions for a strong wind, e.g., $X({\rm C}) \lesssim 0.51$, 0.46 and 0.41, for Z=0.02, 0.01, and 0.004, respectively.

(2) On the other hand, the lower bound, $X({\rm C}) \simeq 0.35 - 0.33$, does not depend much on Z, since it is imposed by the maximum $M_{\rm CO}$.

(3) Assuming the relation between $M_{\rm Ni56}$ and $X({\rm C})$ given in Figure 8, our model predicts the absence of brighter SNe Ia in lower metallicity environment.

3.3.2. *Age effects on the minimum* $M_{\rm WD,0}$

In our model, the age of the progenitor system also constrains the range of $X({\rm C})$ in SNe Ia. In the SD scenario, the lifetime of the binary system is essentially the main-sequence lifetime of the companion star, which depends on its initial mass M_2. HKNU99 and HKN99 have obtained a constraint on M_2 by calculating the evolution of accreting WDs for a set of initial masses of the WD ($M_{\rm WD,0} \simeq M_{\rm CO}$) and of the companion ($M_2$), and the initial binary period (P_0). In order for the WD mass to reach $M_{\rm Ia}$, the donor star should transfer enough material at the appropriate accretion rates. The donors of successful cases are divided into two categories: one is composed of slightly evolved main-sequence stars with $M_2 \sim 1.7 - 3.6 M_\odot$ (for Z=0.02), and the other of red-giant stars with $M_2 \sim 0.8 - 3.1 M_\odot$ (for Z=0.02) (Fig. 4).

If the progenitor system is older than 2 Gyr, it should be a system with a donor star of $M_2 < 1.7 M_\odot$ in the red-giant branch. Systems with $M_2 > 1.7 M_\odot$ become SNe Ia in a time shorter than 2 Gyr. Likewise, for a given age of the progenitor system, M_2 must be smaller than a limiting mass. This constraint on M_2 can be translated into the presence of a minimum $M_{\rm CO}$ for a given age, as follows: For a smaller M_2, i.e. for the older system, the total mass which can be transferred from the donor to the WD is smaller. In order for $M_{\rm WD}$ to reach $M_{\rm Ia}$, therefore, the initial mass of the WD, $M_{\rm WD,0} \simeq M_{\rm CO}$, should be larger. This implies that the older system should have larger minimum $M_{\rm CO}$ as indicated in Figure 8. Using the $X({\rm C})$-$M_{\rm CO}$ and $M_{\rm Ni56}$-$X({\rm C})$ relations (Fig. 8), we conclude that WDs in older progenitor systems have a smaller $X({\rm C})$, and thus produce dimmer SNe Ia.

3.4. *Comparison with observations*

The first observational indication which can be compared with our model is the possible dependence of the SN brightness on the morphology of the host galaxies. Hamuy et al. (1996) found that the most luminous SNe Ia occur in spiral galaxies, while both spiral and elliptical galaxies are hosts to dimmer SNe Ia. Hence, the mean peak brightness is lower in elliptical than in spiral galaxies.

In our model, this property is simply understood as the effect of the different age of the companion. In spiral galaxies, star formation occurs continuously up to the present time. Hence, both WD+MS and WD+RG systems can produce SNe Ia. In elliptical galaxies, on the other hand, star formation has long ended, typically more than 10 Gyr ago. Hence, WD+MS systems can no longer produce SNe Ia. In Figure 9, we show

the frequency of the expected SN I for a galaxy of mass $2 \times 10^{11} M_\odot$ for WD+MS and WD+RG systems separately as a function of $M_{\rm CO}$. Here we use the results of HKN99 and HKNU99, and the $M_{\rm CO} - X({\rm C})$ and $M_{\rm Ni56} - X({\rm C})$ relations given in Figure 8. Since a WD with smaller $M_{\rm CO}$ is assumed to produce a brighter SN Ia (larger $M_{\rm Ni56}$), our model predicts that dimmer SNe Ia occur both in spirals and in ellipticals, while brighter ones occur only in spirals. The mean brightness is smaller for ellipticals and the total SN Ia rate per unit luminosity is larger in spirals than in ellipticals. These properties are consistent with observations.

The second observational suggestion is the radial distribution of SNe Ia in galaxies. Wang et al. (1997) and Riess et al. (1998) found that the variation of the peak brightness for SNe Ia located in the outer regions in galaxies is smaller. This behavior can be understood as the effect of metallicity. As shown in Figure 8, even when the progenitor age is the same, the minimum $M_{\rm CO}$ is larger for a smaller metallicity because of the metallicity dependence of the WD winds. Therefore, our model predicts that the maximum brightness of SNe Ia decreases as metallicity decreases. Since the outer regions of galaxies are thought to have lower metallicities than the inner regions (Zaritsky et al. 1994; Kobayashi & Arimoto 1999), our model is consistent with observations. Wang et al. (1997) also claimed that SNe Ia may be deficient in the bulges of spiral galaxies. This can be explained by the age effect, because the bulge consists of old population stars.

3.5. *Diversity of high redshift supernovae*

We have suggested that $X({\rm C})$ is the quantity very likely to cause the diversity in $M_{\rm Ni56}$ and thus in the brightness of SNe Ia. We have then shown that our model predicts that the brightness of SNe Ia depends on the environment, in a way which is qualitatively consistent with the observations. Further studies of the propagation of the turbulent flame and the DDT are necessary in order to actually prove that $X({\rm C})$ is the key parameter.

Our model predicts that when the progenitors belong to an old population, or to a low metal environment, the number of very bright SNe Ia is small, so that the variation in brightness is also smaller. In spiral galaxies, the metallicity is significantly smaller at redshifts $z \gtrsim 1$, and thus both the mean brightness of SNe Ia and its range tend to be smaller. At $z \gtrsim 2$ SNe Ia would not occur in spirals at all because the metallicity is too low. In elliptical galaxies, on the other hand, the metallicity at redshifts $z \sim 1-3$ is not very different from the present value. However, the age of the galaxies at $z \simeq 1$ is only about 5 Gyr, so that the mean brightness of SNe Ia and its range tend to be larger at $z \gtrsim 1$ than in the present ellipticals because of the age effect.

We note that the variation of $X({\rm C})$ is larger in metal-rich nearby spirals than in high redshift galaxies. Therefore, if $X({\rm C})$ is the main parameter responsible for the diversity of SNe Ia, and if the light curve shape (LCS) method is confirmed by the nearby SNe Ia data, the LCS method can also be used to determine the absolute magnitude of high redshift SNe Ia.

3.6. *Possible evolutionary effects*

In the above subsections, we consider the metallicity effects only on the C/O ratio; this is just to shift the main-sequence mass - $M_{\rm WD,0}$ relation, thus resulting in no important evolutionary effect. However, some other metallicity effects could give rise to evolution of SNe Ia between high and low redshifts (i.e., between low and high metallicities).

Here we point out just one possible metallicity effect on the carbon ignition density in the accreting WD. The ignition density is determined by the competition between the compressional heating due to accretion and the neutrino cooling. The neutrino emission is enhanced by the *local* Urca shell process of, e.g., ^{21}Ne–^{21}F pair (Paczyński 1973). (Note

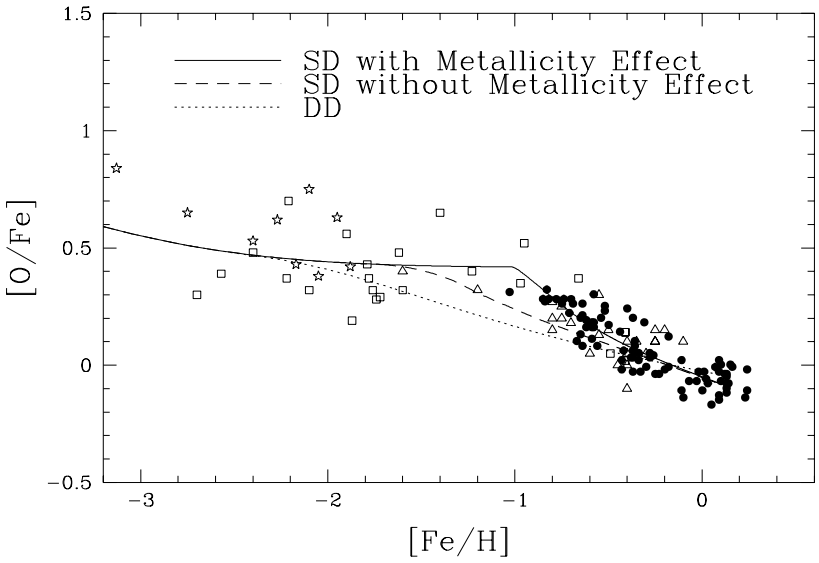

FIGURE 10. The evolutionary change in [O/Fe] against [Fe/H] for three SN Ia models. The dotted line is for the DD scenario, and the other lines are for our SD scenario with (solid line) and without (dashed line) the metallicity effect on SNe Ia. Observational data sources: filled circles, Edvardsson et al. (1993); open triangles, Barbuy & Erdelyi-Mendes (1989); stars, Nissen et al. (1994); open squares, Gratton (1991).

that this is different from the *convective* Urca neutrino process). For higher metallicity, the abundance of ^{21}Ne is larger so that the cooling is larger. This could delay the carbon ignition until a higher central density is reached (Nomoto et al. 1997d).

Since the WD with a higher central density has a larger binding energy, the kinetic energy of SNe Ia tends to be smaller if the same amount of ^{56}Ni is produced. This might cause a systematically slower light curve evolution at higher metallicity environment. The carbon ignition process including these metallicity effects as well as the convective Urca neutrino process need to be studied (see also Iwamoto et al. 1999 for nucleosynthesis constraints on the ignition density).

4. The chemical evolution in the solar neighborhood

The role of SNe II and SNe Ia in the chemical evolution of galaxies can be seen in the [O/Fe]-[Fe/H] relation (Fig. 10: Metal-poor stars with [Fe/H] $\lesssim -1$ have [O/Fe] ~ 0.45 on the average, while disk stars with [Fe/H] $\gtrsim -1$ show a decrease in [O/Fe] with increasing metallicity. To explain such an evolutionary change in [O/Fe] against [Fe/H], we use the chemical evolution model that allows the infall of material from outside the disk region. The infall rate, the SFR, and the initial mass function (IMF) are given by Kobayashi et al. (1998), and the nucleosynthesis yields of SNe Ia and II are taken from Nomoto et al. (1997bc) and Tsujimoto et al. (1995).

The metallicity effects on SNe Ia on the chemical evolution is examined. For the DD scenario, the distribution function of the lifetime of SNe Ia by Tutukov & Yungelson (1994) is adopted, majority of which is $\sim 0.1-0.3$ Gyr. Figure 10 shows the evolutionary change in [O/Fe] for three SN Ia models. The dotted line is for the DD scenario. The other

lines are for our SD scenario with (solid line) and without (dashed line) the metallicity effect on SNe Ia.

(i) In the DD scenario the lifetime of the majority of SNe Ia is shorter than 0.3 Gyr. Then the decrease in [O/Fe] starts at [Fe/H] ~ -2, which is too early compared with the observed decrease in [O/Fe] starting at [Fe/H] ~ -1.

(ii) For the SD scenario with no metallicity effect, the companion star with $M \sim 2.6 M_\odot$ evolves off the main-sequence to give rise to SNe Ia at the age of ~ 0.6 Gyr. The resultant decrease in [O/Fe] starts too early to be compatible with the observations.

(iii) For the metallicity dependent SD scenario, SNe Ia occur at [Fe/H] $\gtrsim -1$, which naturally reproduce the observed break in [O/Fe] at [Fe/H] ~ -1. Also the low-metallicity inhibition of SN Ia provides a new interpretation of the SN II-like abundance patterns of the Galactic halo and the DLA systems (Kobayashi et al. 1998).

5. Cosmic supernova rates

Attempts have been made to predict the cosmic supernova rates as a function of redshift by using the observed cosmic star formation rate (SFR) (Ruiz-Lapuente & Canal 1998; Sadat et al. 1998; Yungelson & Livio 1998). The observed cosmic SFR shows a peak at $z \sim 1.4$ and a sharp decrease to the present (Madau et al. 1996). However, UV luminosities which is converted to the SFRs may be affected by the dust extinction (Pettini et al. 1998). Recent updates of the cosmic SFR suggest that a peak lies around $z \sim 3$.

Kobayashi et al. (1998) predicts that the cosmic SN Ia rate drops at $z \sim 1-2$, due to the metallicity-dependence of the SN Ia rate. Their finding that the occurrence of SNe Ia depends on the metallicity of the progenitor systems implies that the SN Ia rate strongly depends on the history of the star formation and metal-enrichment. The universe is composed of different morphological types of galaxies and therefore the cosmic SFR is a sum of the SFRs for different types of galaxies. As each morphological type has a unique star formation history, we should decompose the cosmic SFR into the SFR belonging to each type of galaxy and calculate the SN Ia rate for each type of galaxy.

Here we first construct the detailed evolution models for different type of galaxies which are compatible with the stringent observational constraints, and apply them to reproduce the cosmic SFR for two different environments, e.g., the cluster and the field. Secondly with the self-consistent galaxy models, we calculate the SN rate history for each type of galaxy and predict the cosmic supernova rates as a function of redshift. We adopt $H_0 = 50$ km s^{-1} Mpc^{-1}, $\Omega_0 = 0.2$, $\lambda_0 = 0$ and the galactic age of 15 Gyr for a standard model, which corresponds to the redshift at the formation epoch of galaxies $z_{\rm f} \sim 5$.

5.1. *Supernova rates and galaxy types*

We assume that elliptical galaxies are formed by a single star burst and stop the star formation at $t \sim 1$ Gyr due to the supernova-driven galactic wind (e.g., Kodama & Arimoto 1997), while spiral galaxies are formed by a relatively continuous star formation. These models can well reproduce the present gas fractions, colors, supernova rates, and the color evolution in cluster ellipticals (see Figures 11 and 12).

Present supernova rates observed in the various type of galaxies (Cappellaro et al. 1997) put the constraints on the SN Ia progenitor models. Using the galaxy model shown in Figures 11 and 12, we show that our SN Ia model well reproduces the present supernova rates in both spirals and ellipticals (Kobayashi et al. 1999).

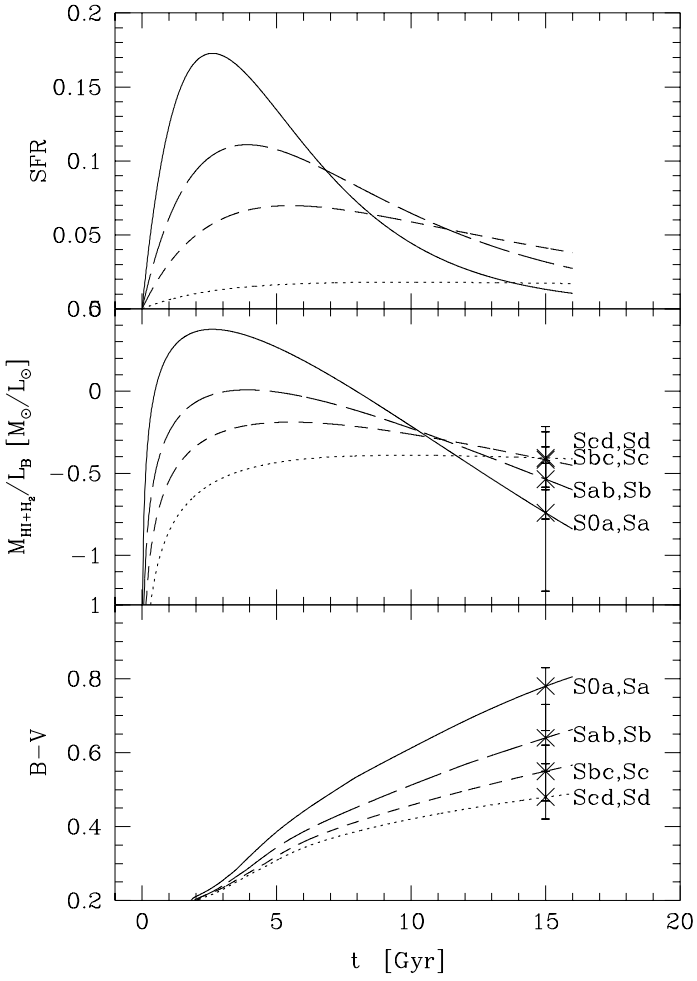

FIGURE 11. The star formation rates (top panel) gas fractions (middle panel) and the $B-V$ colors (bottom panel) in four types of spirals : S0a-Sa (solid line), Sab-Sb (long-dashes line), Sbc-Sc (short-dashed line), and Scd-Sd (dotted line). The present B-V colors are taken from Roberts & Haynes (1994), and the present gas fractions are normalized by the present blue luminosities and are derived from HI fractions (Roberts & Haynes 1994) and H_2/HI ratios (Casoli et al. 1998).

5.1.1. *Spiral galaxies*

The observed SN II rate $\mathcal{R}_{\rm II}$ in late-type spirals is about twice the rate in early-type spirals. On the other hand, the observed SN Ia rate $\mathcal{R}_{\rm Ia}$ in both types of spirals are nearly the same. Therefore the present $\mathcal{R}_{\rm Ia}/\mathcal{R}_{\rm II}$ ratio in early-type spirals is about twice that in late-type spirals. Such a difference in the relative frequency is a result of the difference in the SFR, because the dependences of $\mathcal{R}_{\rm II}$ and $\mathcal{R}_{\rm Ia}$ on the SFR are different due to the different lifetimes of supernova progenitors. Therefore the observed $\mathcal{R}_{\rm Ia}/\mathcal{R}_{\rm II}$ ratio gives a constraint on the SN Ia progenitor model.

In the DD scenario, the lifetime of majority of SNe Ia is $\sim 0.1 - 0.3$ Gyr, so that the evolution of $\mathcal{R}_{\rm Ia}$ is similar to that of $\mathcal{R}_{\rm II}$. Therefore $\mathcal{R}_{\rm Ia}/\mathcal{R}_{\rm II}$ is insensitive to the SFR.

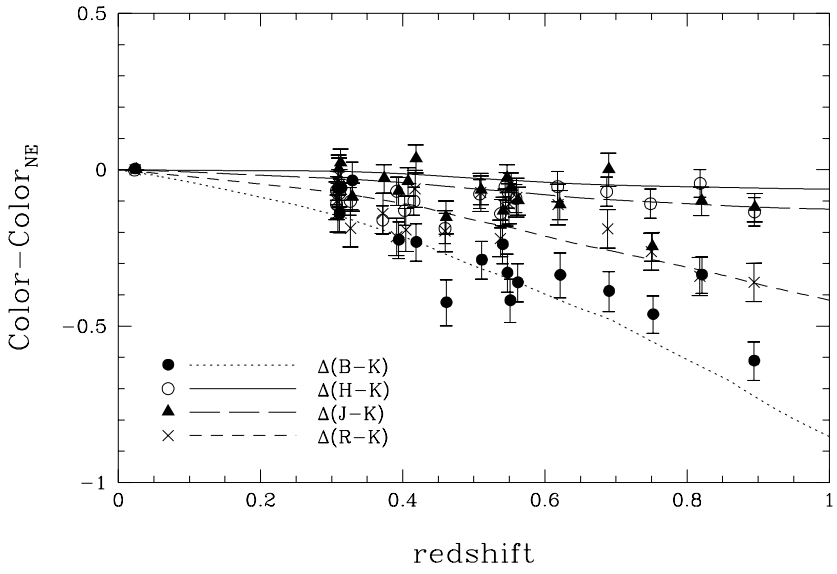

FIGURE 12. The passive color evolution of cluster ellipticals up to $z \sim 1$. The observational data are taken from Stanford et al. (1998).

This results in the small differences in $\mathcal{R}_{\rm Ia}/\mathcal{R}_{\rm II}$ among the various type of spirals, which is not consistent with observations.

In our SN Ia model, if the iron abundance of progenitors is [Fe/H]$\gtrsim -1$, the occurrence of SNe Ia is determined from the lifetime of the companions. If SNe Ia would occur only in the MS+WD systems with relatively short lifetimes, $\mathcal{R}_{\rm Ia}/\mathcal{R}_{\rm II}$ would have been insensitive to the SFR. On the contrary, if SNe Ia would occur only in the RG+WD systems with long lifetimes, the present difference in $\mathcal{R}_{\rm Ia}/\mathcal{R}_{\rm II}$ between early and late type spirals would have been too large, reflecting the large difference in SFR at an early epoch. Owing to the presence of these two types of the progenitor systems in our SN Ia progenitor model, the observed difference in $\mathcal{R}_{\rm Ia}/\mathcal{R}_{\rm II}$ can be reproduced.

5.1.2. *Elliptical galaxies*

We assume that a bulk of stars in cluster ellipticals are formed at $z \gtrsim 3$, and have ages $\gtrsim 10$ Gyr. In the DD scenario, the SN Ia lifetimes are mostly so short as $t_{\rm Ia} \lesssim 0.3$ Gyr that too few SNe Ia occur at the present epoch. Our SN Ia model includes the WD+RG systems with $t_{\rm Ia} \gtrsim 10$ Gyr, thus well reproducing the present SNe Ia rate in ellipticals.

From $z \sim 0.2$ to $z \sim 0$, the SN Ia rate gradually decreases to the present by $\sim 20\%$. This is due to the smallest companions with $0.9 M_\odot$ to produce SNe Ia, which give the longest SN Ia lifetime of ~ 11 Gyr for $Z = 0.002$ and ~ 18 Gyr for $Z = 0.02$. As the star formation in ellipticals has been stopped more than 10 Gyr before, majority of SN Ia progenitors with $Z = 0.002$ have already explode and only metal-rich SNe Ia occurs at $z \sim 0$. The decrease in the SN Ia rate from $z \sim 0.2$ to $z \sim 0$ also depends on the star formation history in ellipticals and the galactic age. If ellipticals have undergone the relatively continuous star formation, as suggested by the hierarchical clustering simulations, the SN Ia rate might keep constant to the present.

5.2. *Cosmic supernova rates*

We calculate the cosmic supernova rate by summing up the rates of spirals and ellipticals with the ratio of the relative mass contribution among the types. The relative mass contribution is given by the observed relative luminosity proportion for ellipticals, S0a-Sa, Sab-Sb, Sbc-Sc, and Scd-Sd (Pence 1976) and the calculated mass to light ratio in B-band. We adopt the the initial comoving density of gas $\Omega_{g\infty} = 3.5 \times 10^{-3} h^{-1}$.

5.2.1. *In clusters*

First, we make a prediction of the cosmic supernova rates in the cluster galaxies using the galaxy models which are in good agreements with the observational constraints (Figs. 11 and 12). The upper panel of Figure 13 shows the cosmic SFR (solid line) as a composite of spirals (long-dashed line) and ellipticals (short-dashed line).

In our galaxy models, ellipticals undergo a star burst at $z \gtrsim 3$ and the duration of the star formation is ~ 1 Gyr, while spirals undergo relatively continuous star formation. Thus, only the SFR in spirals is responsible for the cosmic SFR at $z \lesssim 2$. For reference, the observed cosmic SFR in field, so-called Madau's plot, is also plotted. Compared with them, the predicted cosmic SFR has a little shallower slope from the present to the peak at $z \sim 1.4$ (see also Totani et al. 1997). The high SFR in ellipticals appears at $z \gtrsim 3$. Such ellipticals may be hidden by the dust extinction (Pettini et al. 1998) or may have formed at $z \sim 5$ (Totani et al. 1997).

The chemical enrichment in ellipticals has taken place with so much shorter timescale that the iron abundance reaches [Fe/H] ~ -1 at $z \gtrsim 4$ and the metallicity effect on SNe Ia does not appear. In spirals, the iron abundance reaches [Fe/H] ~ -1 at $z \sim 2.3$.

The lower panel of Figure 13 shows the cosmic supernova rates (solid line) as a composite of spirals (long-dashed line) and ellipticals (short-dashed line). The upper and lower three lines show the SN II and Ia rates, respectively. Our SN Ia model can successfully reproduce the observed rate at $z \sim 0.5$ (Pain et al. 1996, filled circle; Pain 1999, filled square).

The SN Ia rate in spirals drops at $z \sim 2$ because of the low-metallicity inhibition of SNe Ia. In ellipticals, the chemical enrichment takes place so early that the metallicity is large enough to produce SNe Ia at $z \gtrsim 3$. Thus, the SN Ia rate depends almost only on the lifetime. A burst of SNe Ia occurs after ~ 0.5 Gyr from the beginning of the star formation which corresponds to the shortest lifetime of the WD+MS binaries; this forms a peak of the SN Ia rate at $z \sim 2.5$. The second peak of the SN Ia rate appears at $z \sim 1.5$ (~ 2 Gyr) due to the beginning of the explosions of SNe Ia from WD+RG binaries. If SNe Ia at $z \gtrsim 2$ are observed with their host galaxies using the Next Generation Space Telescope, we can precisely test the metallicity effect by finding the drop of SN Ia rate in spirals.

The cosmic SN Ia rate using the observed cosmic SFR drops at $z \sim 1.6$ ($z \sim 1.2$ in Kobayashi et al. 1998). This is because the chemical enrichment of the whole universe is much slower than in spirals and ellipticals.

5.2.2. *In fields*

The observed spectra of ellipticals in the Hubble Deep Field suggest that the formation of ellipticals is protracted in fields, that is, the formation epochs of ellipticals span in the wide range of redshifts of $1 \lesssim z \lesssim 4$ (Franceschini et al. 1998). We also predict the cosmic supernova rates for this case, assuming the distribution function of formation epochs to meet Franceschini's et al. (1998) results.

The upper panel of Figure 14 shows the cosmic SFR (solid line) as a composite of spirals (long-dashed line) and field ellipticals (short-dashed line).

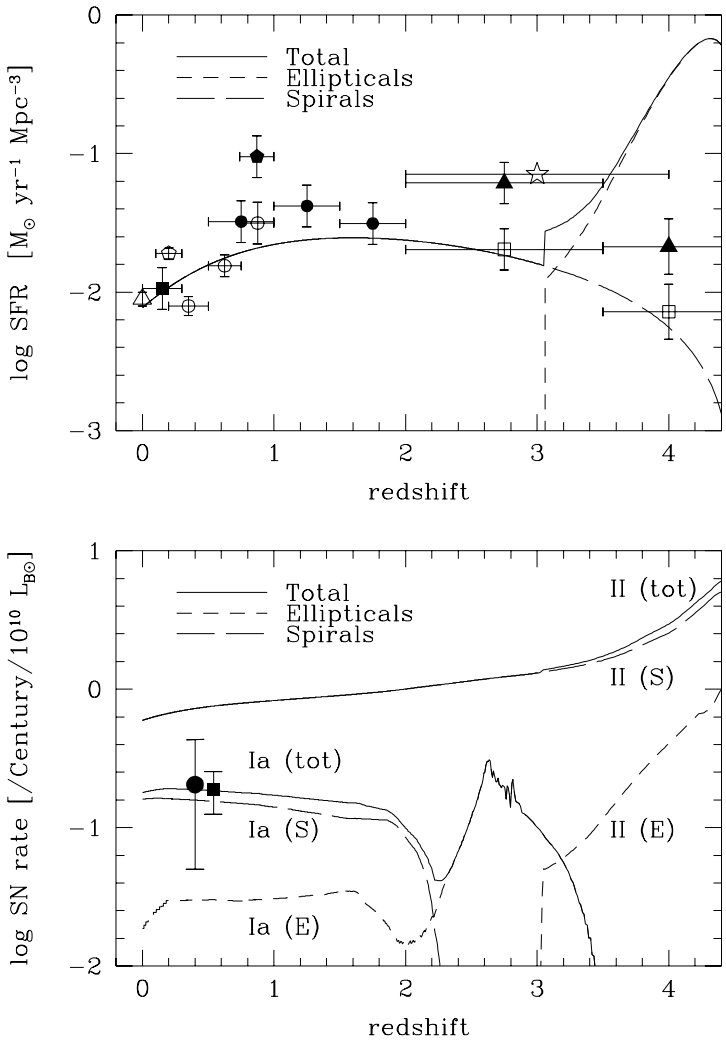

FIGURE 13. The upper panel shows the cosmic SFR (solid line) as a composite of spirals (long-dashed line) and ellipticals (short-dashed line). The dots are the observational data (Gallego et al. 1995, open triangle; Lilly et al. 1996, open circles; Madau et al. 1996, open squares; Connolly et al. 1997, filled circles; Tresse & Maddox 1998, open pentagon; Treyer et al. 1998, filled square; Glazebrook et al. 1999, filled pentagon; Hughes et al. 1998, star; Pettini et al. 1998, filled triangle). The lower panel shows the cosmic supernova rate (solid line) as a composite of spirals (long-dashed line) and ellipticals (short-dashed line). The observational data are from Pain et al. (1996) and Pain (1999).

The SFR in spirals is the same as in the upper panel of Figure 13, but the star formation in ellipticals continues to the present on the average. The peak of the star formation is at $z \sim 3$, which is consistent with the recent sub-mm data (Hughes et al. 1998). The synthesized cosmic SFR can successfully reproduce the observed one, except for the recent Hα data (Glazebrook et al. 1999).

The lower panel of Figure 14 shows the cosmic supernova rates (solid line) as a com-

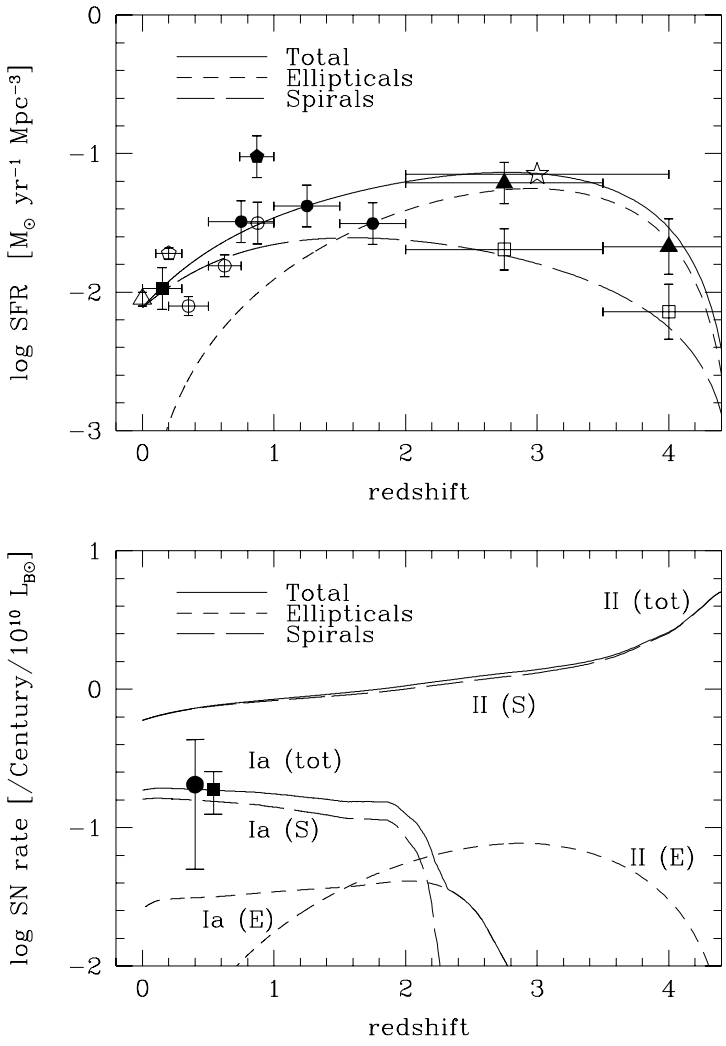

FIGURE 14. The same as Figure 13, but for the formation epochs of ellipticals spanning over $1 \lesssim z \lesssim 4$, which might correspond to field ellipticals.

posite of spirals (long-dashed line) and ellipticals (short-dashed line). The upper and lower three lines show the SN II and Ia rates, respectively.

The SN Ia rate in spirals drops at $z \sim 2$ as in the lower panel of Figure 13. Contrary to Figure 13, the SN Ia rate in field ellipticals gradually decreases from $z \sim 2$ to $z \sim 3$, which is not due to the metallicity effect but due to the lifetime effect. Although the chemical enrichment timescale in each elliptical is as fast as in the lower panel of Figure 13, the star formation averaged over whole ellipticals takes place more gradually, and the number of stars becomes smaller toward higher redshifts.

In this case, SNe II may be observed in low-redshift ellipticals. The different SN II and Ia rates between cluster and field ellipticals reflects the difference in the star formation histories in different environments.

5.2.3. *Summary*

We make a prediction of the cosmic supernova rate history as a composite of the different types of galaxies. We adopt the SN Ia progenitor scenario including the metallicity effect proposed by Kobayashi et al. (1998), which can successfully reproduce the chemical evolution of the solar neighborhood. To calculate the comic SFR, we construct the galaxy evolution models for spirals and ellipticals to meet the observational constraints such as the present gas fractions and colors for spirals, and the mean stellar metallicity and the color evolution from the present to $z \sim 1$ for ellipticals.

Owing to the *two* types of the progenitor system (MS+WD and RG+WD), i.e., shorter $(0.6 - 1$ Gyr) and longer lifetimes $(2 - 15$ Gyr) of SN Ia progenitors, we can explain the moderate contrast of the relative ratio of SN Ia to SN II rate $\mathcal{R}_{\rm Ia}/\mathcal{R}_{\rm II}$ between the early and late types of spirals. Owing to over 10 Gyr lifetime of the RG+WD systems, SNe Ia can be seen even at the present in ellipticals where the star formation has already stopped over 10 Gyr before.

Then we construct the cosmic SFR as the composite of the SFR for different types of galaxies, and predict the cosmic supernova rates:

(*a*) In the cluster environment, the synthesized cosmic SFR has an excess at $z \gtrsim 3$ corresponding to the SFR in ellipticals and a shallower slope from the present to the peak at $z \sim 1.4$, compared with Madau's plot. The predicted cosmic supernova rate suggests that SNe Ia can be observed even at high redshifts because the chemical enrichment takes place so early that the metallicity is large enough to produce SNe Ia at $z \gtrsim 3$ in cluster ellipticals. In spirals the SN Ia rate drops at $z \sim 2$ because of the low-metallicity inhibition of SNe Ia.

(*b*) In the field environment, ellipticals are assumed to form at such a wide range of redshifts as $1 \lesssim z \lesssim 4$. The synthesized cosmic SFR has a broad peak around $z \sim 3$, which well reproduces the observed one. The SN Ia rate is expected to be significantly low at $z \gtrsim 2$ because the SN Ia rate drops at $z \sim 2$ in spirals and gradually decreases from $z \sim 2$ in ellipticals.

This work has been supported in part by the grant-in-Aid for COE Scientific Research (07CE2002) of the Ministry of Education, Science, Culture and Sports in Japan.

REFERENCES

Arnett, W.D. 1996, Nucleosynthesis and Supernovae (Princeton: Princeton Univ. Press)

Barbuy, B., & Erdelyi-Mendes, M. 1989, A&A214 239

Branch, D. 1998, ARA&A, 1998, 36, 17

Branch, D., Lacy, C.H., McCall, M.L., Sutherland, P., Uomoto, A., Wheeler, J.C., & Wills, B.J. 1983, ApJ, 270, 123

Branch, D., Livio, M., Yungelson, L. R., Boffi, F. R., & Baron, E. 1995, PASP, 107, 717

Branch, D., Romanishin, W., & Baron, E., 1996, ApJ, 465, 73

Cappellaro, E., Turatto, M., Tsvetkov, D. Yu., Bartunov, O.S., Pollas, C., Evans, R., & Hammuy, M., 1997, A&A, 322, 431

Casoli, F., Sauty, S., Gerin, M., Boselli, A., Fouqué, P., Braine, J., Gavazzi, G., Lequeux, J., & Dickey, J. 1998, A&A, 331, 451

Connolly, A. J., Szalay, A. S., Dickinson, M., SubbaRao, M. U., & Brunner, R. J. 1997, ApJ, 486, L11

Cumming, R.J., Lundqvist, P., Smith, L.J., Pettini, M., & King, D.L. 1996, MNRAS, 283, 1355

Eck, C.R., Cowan, J.J., Roberts, D.A., Boffi, F.R., & Branch, D. 1995, ApJ, 451, L53

Edvardsson, B., Andersen, J., Gustafsson, B., Lambert, D. L., Nissen, P. E., & Tomkin, J. 1993, A&A, 275, 101

Franceschini, A., Silva, L., Fasano, G., Granato, G. L., Bressan, A., Arnouts, S. & Danese, L. 1998, ApJ, 506, 600

Gallego, J., Zamorand, J., Aragón-Salamanca, A., & Rego, M. 1995, ApJ, 455, L1

Garnavich, P. et al. , 1998, ApJ, 493, 53

Gilliland, R. L., Nugent, P. E., & Phillips, M. M. 1999, ApJ, in press (astro-ph/9903229)

Glazebrook, K., Blake, C., Economou, F., Lilliy S., & Colles, M. 1999, MNRAS, 306, 843

Gratton, R. G. 1991, in IAU Symp. 145, Evolution of Stars: The Photometric Abundance Connection, ed. G. Michaud & A. V. Tutukov (Montreal: Univ. Montreal), 27

Hachisu, I., & Kato, M., 1999, in preparation

Hachisu, I., Kato, M., & Nomoto, K., 1996, ApJ, 470, L97

Hachisu, I., Kato, M., & Nomoto, K. 1999, ApJ, 522, 487

Hachisu, I., Kato, M., Nomoto, K., & Umeda, H. 1999, ApJ, 519, 314

Hamuy, M., et al. 1995, AJ, 109, 1

Hamuy, M., Phillips, M. M., Schommer, R. A., & Suntzeff, N. B., 1996, AJ, 112, 2391.

Höflich, P., & Khokhlov, A., 1996, ApJ, 457, 500

Höflich, P., Nomoto, K., Umeda, H., & Wheeler, J. C., 1999, ApJ, in press

Höflich, P., Wheeler, J. C., & Thielemann, F. -K., 1998, ApJ, 495, 617

Hughes, D., et al. 1998, Nature, 394, 241

Iben, I. Jr., & Tutukov, A. V. 1984, ApJS, 54, 335

Iglesias, C. A., & Rogers, F. 1993, ApJ, 412, 752

Iwamoto, K., Brachwitz, F., Nomoto, K., Kishimoto, N., Umeda, H., Hix, W. R., Thielemann, F-K. 1999, ApJS, 125, in press

Kato, M., & Hachisu, I., 1999, ApJ, 513, L41

Khokhlov, A. 1991, A&A, 245, 114

Kobayashi, C., & Arimoto, N. 1999, ApJ, 526, in press

Kobayashi, C., Tsujimoto, T., & Nomoto, K. 1999, ApJ, submitted

Kobayashi, C., Tsujimoto, T., Nomoto, K., Hachisu, I, & Kato, M. 1998, ApJ, 503, L155

Kodama, T., & Arimoto, N., 1997, A&A, 320, 41

Kodama, T., Bower, R. G., & Bell, E. F. 1999, MNRAS, 306, 561

Li, X.-D., & van den Heuvel, E.P.J., 1997, A&A, 322, L9

Lilly, S. J., Le Fèvre, O., Hammer, F., & Crampton, D. 1995, ApJ, 460, L1

Madau, P., Ferguson, H. C., Dickinson, M. E., Giavalisco, M., Steidel, C. C., & Fruchter, A. 1996, MNRAS, 283, 1388

Mazzali, P. A., Cappellaro, E., Danziger, I. J., Turatto, M., & Benetti, S., 1998, ApJ, 499, L49

Niemeyer J.C., & Hillebrandt W. 1995, ApJ, 452, 769

Nissen, P. E., Gustafsson, B., Edvardsson, B., & Gilmore, G. 1994, A&A, 285, 440

Nomoto, K., 1982, ApJ, 253, 798

Nomoto, K., Iwamoto, K., & Kishimoto, N. 1997a, Science, 276, 1378

Nomoto, K., Hashimoto, M, Tsujimoto, T, Thielemann, F.-K, Kishimoto, N., Kubo, Y., & Nakasato, N. 1997b, Nuclear Physics, A616, 79c

Nomoto, K., Iwamoto, K., Nakasato, N., Thielemann, F.-K, Brachwitz, F., Tsujimoto, T., Kubo, Y., & Kishimoto, N. 1997c, Nuclear Physics, A621, 467c

Nomoto, K., et al. 1997d, in Thermonuclear Supernovae, Eds. P.Ruiz-Lapuente et al. (Dordrecht: Kluwer), 349

Nomoto, K., & Kondo, Y., 1991, ApJ, 367, l19

Nomoto, K., Nariai, K., & Sugimoto, D., 1979, PASJ, 31, 287

Nomoto, K., Thielemann, F. -K., & Yokoi, K., 1984, ApJ, 286, 644

Nomoto, K., Yamaoka, H., Shigeyama, T., Kumagai, S., & Tsujimoto, T. 1994, in Supernovae, Les Houches Session LIV, ed. S. A. Bludman et al. (Amsterdam: North-Holland), 199

Nugent, P., Baron, E., Branch, D., Fisher, A., & Hauschildt, P. H. 1997, ApJ, 485, 812

Paczyński, B. 1973, Acta Astr. 23, 1

Pain, R. 1999, Talk at the Type Ia supernova workshop in Aspen

Pain, R., et al. 1996, ApJ, 473, 356

Pei, Y. C., & Fall, S. M., 1995, ApJ, 454, 69

Pei, Y. C., Fall, S. M., & Hauser, M. G. 1999, ApJ, in press

Pence, W. 1976, ApJ, 420, L1

Perlmutter, S. et al. 1997, ApJ, 483, 565

Perlmutter, S. et al. 1999, ApJ, 517, 565

Pettini, M., Kellogg, M.,Steidel, C. C., Dickinson, M., Adelberger, K. L, & Giavalisco, M. 1998, ApJ, 508, 539

Phillips, M. M., 1993, ApJ, 413, L75

Riess, A.G., Press, W.H., & Kirshner, R.P. 1995, ApJ, 438, L17

Riess, A.G. et al. 1998, AJ, 116, 1009

Riess, A. G. et al. 1999, AJ, 117, 707

Roberts M. S. & Haynes M. P. 1994, ARAA, 32, 115

Ruiz-Lapuente, P., & Canal, R. 1998, ApJ, 497, L57

Sadat, R., Blanchard, A., Guiderdoni, B., & Silk, J. 1998, A&A, 331, L69

Saio, H., & Nomoto, K. 1985, A&A, 150, L21

Saio, H., & Nomoto, K. 1998, ApJ, 500, 388

Sandage, A., & Tammann, G.A., 1993, ApJ, 415, 1

Schlegel, E.M., & Petre, R. 1993, ApJ, 418, L53

Segretain, L., Chabrier, G., & Mochkovitch, R. 1997, ApJ, 481, 355

Stanford, S.A., Eisenhardt, P.R.M., & Dickinson, M., 1998, ApJ, 492, 461

Suzuki, T., & Nomoto, K. 1995, ApJ, 455, 658

Totani, T., Yoshii, Y., & Sato, K. 1997, ApJ, 483, L75

Tresse, L., & Maddox, S. J. 1998, ApJ, 495, 691

Treyer, M. A., Ellis, R. S., Milliard, B., Donas, J., & Bridges, T. J. 1998, MNRAS, 300, 303

Tsujimoto, T., Nomoto, K., Yoshii, Y., Hashimoto, M., Yanagida, S., & Thielemann, F.-K. 1995, MNRAS, 277, 945

Tutukov, A. V., & Yungelson, L. R. 1994, MNRAS, 268, 871

Umeda, H., Nomoto, K., Ymamaoka, H., & Wanajo, S. 1999a, ApJ, 513, 861

Umeda, H., Nomoto, K., Kobayashi, C., Hachisu, I, & Kato, M. 1999b, ApJL, 522, in press (astro-ph/9906192)

van den Heuvel, E.P.J., 1994, in Interacting Binaries, eds. S.N. Shore et al. (Berlin: Springer-Verlag), 263

van den Heuvel, E. P. J., Bhattacharya, D., Nomoto, K., & Rappaport, S. 1992, A&A, 262, 97

Wang, L., Höflich, P., & Wheeler, J. C. 1997, ApJ, 483, L29

Webbink, R. F. 1984, ApJ, 277, 355

Yungelson, L., & Livio, M. 1998, ApJ, 497, 168

Zaritsky, D., Kennicutt, R.C., & Huchra, J.P. 1994, ApJ, 420, 87